AGU PUBLICATIONS

Global Biogeochemical Cycles

RESEARCH ARTICLE
10.1002/2015GB005124

Key Points:
- Most of river Hg discharged to ocean is refractory
- Long-range transport of riverine Hg is enhanced by major ocean currents
- Circumpolar rivers carry more reactive Hg

Supporting Information:
- Figure S1

Correspondence to:
Y. Zhang,
yxzhang@seas.harvard.edu

Citation:
Zhang, Y., D. J. Jacob, S. Dutkiewicz, H. M. Amos, M. S. Long, and E. M. Sunderland (2015), Biogeochemical drivers of the fate of riverine mercury discharged to the global and Arctic oceans, *Global Biogeochem. Cycles*, *29*, doi:10.1002/2015GB005124.

Received 23 FEB 2015
Accepted 30 MAY 2015
Accepted article online 2 JUN 2015

Biogeochemical drivers of the fate of riverine mercury discharged to the global and Arctic oceans

Yanxu Zhang[1], Daniel J. Jacob[1], Stephanie Dutkiewicz[2], Helen M. Amos[3], Michael S. Long[1], and Elsie M. Sunderland[1,3]

[1]Harvard John A. Paulson School of Engineering and Applied Science, Cambridge, Massachusetts, USA, [2]Department of Earth, Atmospheric and Planetary Sciences, Massachusetts Institute of Technology, Cambridge, Massachusetts, USA, [3]Department of Environmental Health, Harvard T. H. Chan School of Public Health, Boston, Massachusetts, USA

Abstract Rivers discharge 28 ± 13 Mmol yr^{-1} of mercury (Hg) to ocean margins, an amount comparable to atmospheric deposition to the global oceans. Most of the Hg discharged by rivers is sequestered by burial of benthic sediment in estuaries or the coastal zone, but some is evaded to the atmosphere and some is exported to the open ocean. We investigate the fate of riverine Hg by developing a new global 3-D simulation for Hg in the Massachusetts Institute of Technology ocean general circulation model. The model includes plankton dynamics and carbon respiration (DARWIN project model) coupled to inorganic Hg chemistry. Results are consistent with observed spatial patterns and magnitudes of surface ocean Hg concentrations. We use observational constraints on seawater Hg concentrations and evasion to infer that most Hg from rivers is sorbed to refractory organic carbon and preferentially buried. Only 6% of Hg discharged by rivers (1.8 Mmol yr^{-1}) is transported to the open ocean on a global basis. This fraction varies from a low of 2.6% in East Asia due to the barrier imposed by the Korean Peninsula and Japanese archipelago, up to 25% in eastern North America facilitated by the Gulf Stream. In the Arctic Ocean, low tributary particle loads and efficient degradation of particulate organic carbon by deltaic microbial communities favor a more labile riverine Hg pool. Evasion of Hg to the Arctic atmosphere is indirectly enhanced by heat transport during spring freshet that accelerates sea ice melt and ice rafting. Discharges of 0.23 Mmol Hg yr^{-1} from Arctic rivers can explain the observed summer maximum in the Arctic atmosphere, and this magnitude of releases is consistent with recent observations. Our work indicates that rivers are major contributors to Hg loads in the Arctic Ocean.

1. Introduction

Consumption of coastal and oceanic fish is the main source of human exposure to the neurotoxin methylmercury that is formed from inorganic divalent mercury (Hg^{II}) [*Sunderland*, 2007]. Globally, rivers discharge 28 ± 13 Mmol yr^{-1} of mercury (Hg) to the ocean margins [*Amos et al.*, 2014], an amount comparable to inputs from atmospheric deposition (10–29 Mmol yr^{-1}) to the global ocean [*Sunderland and Mason*, 2007]. Most of this riverine Hg is buried in ocean margin sediment by particle settling on short time scales [*Chester*, 2003], but some is exported to the open ocean. The magnitude of Hg exported by rivers affects the substrate available for conversion to bioavailable methylmercury in coastal ecosystems and the ocean and thus needs to be accurately quantified. Differences in the geochemical forms of Hg present in the marine environment affect removal from the water column, redox processes, and bioavailability for methylation [*Hsu-Kim et al.*, 2013; *Jonsson et al.*, 2014]. Here we use a global 3-D chemical transport model for oceanic Hg to investigate how ocean transport and interactions between Hg and particulate organic carbon (POC) affect the fate of river-derived Hg.

Most of the Hg in aquatic systems is present as Hg^{II}, which sorbs strongly to POC [*Morel et al.*, 1998]. The affinity of Hg^{II} for suspended particles and other ligands, determined in large part by the composition of POC, has a strong influence on the fate of river-derived Hg since particulate Hg more rapidly deposits to benthic sediments. A large fraction (typically >80%) of the Hg in rivers is in the particulate phase [*Emmerton et al.*, 2013; *Schuster et al.*, 2011]. Dissolved Hg is defined as the filter-passing fraction (<0.2–0.45 μm) and includes Hg^{II} complexes with dissolved organic carbon (DOC), hydroxides, and chlorides.

The stability of Hg^{II} complexes influences the pool available for reduction and methylation. For example, high-molecular-weight organic matter complexes appear to be more resistant to redox transformations

and have limited bioavailability to methylating microbes, likely due to difficulties passing through the cell membrane [*Hsu-Kim et al.*, 2013; *Ravichandran*, 2004; *Whalin et al.*, 2007]. Prior modeling studies have represented Hg^{II} sorption to particles in the open ocean as an equilibrium partitioning process dependent on the concentration of suspended particulate matter [*Soerensen et al.*, 2010; *Zhang et al.*, 2014a]. However, recent field observations suggest major differences in reactivity and desorption kinetics between recently formed Hg^{II}-organic carbon complexes and those with more refractory organic carbon pools [*Hintelmann et al.*, 2002; *Oswald et al.*, 2014]. A more realistic parameterization of marine Hg^{II} speciation is therefore necessary.

Here we use the Massachusetts Institute of Technology (MIT) ocean general circulation model (MITgcm) [*Marshall et al.*, 1997] coupled with a biogeochemistry and ecosystem model (DARWIN project) [*Dutkiewicz et al.*, 2012] to track the geochemical forms and transport of Hg. We apply the model to study the fate of Hg discharges from rivers including exchange between the particulate and dissolved phases facilitated by organic carbon degradation. We evaluate model results using observed Hg concentrations and fluxes as constraints and discuss implications for the importance of riverine Hg loads on a global and regional basis.

We also include a focused analysis of the Arctic Ocean, using a high-resolution one-way nested Arctic simulation of the MITgcm. The Arctic Ocean is of particular interest for Hg because of the dependence of indigenous populations on the ocean as a food source [*Stow et al.*, 2011]. It is a relatively small and shallow ocean with large river inputs [*Opsahl et al.*, 1999]. *Fisher et al.* [2012] suggested that a large Hg flux of 0.47 Mmol yr^{-1} from Arctic rivers and coastal erosion could provide the dominant source of Hg to the Arctic Ocean, as needed to explain a summertime rebound in atmospheric Hg driven by enhanced oceanic evasion. Subsequent research [*Amos et al.*, 2014; *Dastoor and Durnford*, 2014] indicated that the Hg discharges from rivers postulated by *Fisher et al.* [2012] were too large. Here we use our enhanced oceanic modeling capability to determine if a smaller riverine Hg source can be reconciled with the observed summertime rebound in atmospheric Hg.

2. Model Description

We developed a simulation of Hg transport, redox chemistry, and exchange of Hg species between the dissolved and particulate phases within the MIT general circulation model (MITgcm) [*Marshall et al.*, 1997]. The model is configured with a horizontal resolution of $1° \times 1°$ and 23 vertical levels over the global domain except for the Arctic Ocean [*Marshall et al.*, 1997]. Advection and turbulent diffusion is driven by ocean circulation data from the Estimating the Circulation and Climate of the Ocean-Global Ocean Data Assimilation Experiment state estimates (ECCO-GODAE) [*Wunsch and Heimbach*, 2007].

For the Arctic Ocean, we use a separate simulation with a coupled sea ice model. The model employs a cubed-sphere grid that has a horizontal resolution of 36 km and 50 vertical layers [*Heimbach et al.*, 2010; *Losch et al.*, 2010]. The simulation uses prescribed boundary conditions for the Atlantic and Pacific Oceans [*Menemenlis et al.*, 2005] with surface forcing by the atmosphere from the National Center for Environmental Prediction reanalysis [*Kalnay et al.*, 1996] and river freshwater runoff from *Dai and Trenberth* [2002]. The boundary conditions for biogeochemical tracers and Hg are from the global domain model as described above.

We run the model for 30 years with repeated ocean circulation data for the year 2000. The thirtieth simulated year is used for analysis. The initialization time period is sufficiently long for the surface ocean (0–50 m) to achieve a steady state and for riverine sources to be carried to the open ocean by surface currents [*Manizza et al.*, 2009].

We use a coupled simulation of the biogeochemical cycle of organic carbon and associated marine plankton ecosystem (the DARWIN project: http://darwinproject.mit.edu/) within the MITgcm [*Dutkiewicz et al.*, 2012]. This simulation captures the cycling of carbon, nitrogen, silica, phosphorus, and iron through inorganic forms, living plankton (phyto and zoo), and dead organic matter. It computes DOC and POC concentrations, remineralization rates of DOC and POC, and POC sinking fluxes. We also consider the flux of nutrients from rivers (including nitrogen, phosphorus, silica, and carbon) based on the Global Nutrient Export from WaterSheds 2 (NEWS2) data set [*Mayorga et al.*, 2010] and their impact on DOC, POC, and

remineralization. The DARWIN simulation tracks remineralization of labile DOC pools (lifetime of a month). We include more recalcitrant DOC pools (slower remineralization rates) in our Hg simulation by adding the climatological reanalysis data set by *Hansell et al*. [2009] for DOC with lifetimes between 3 and 15,000 years.

We parameterize oceanic Hg chemistry based on the offline global 3-D ocean tracer (OFFTRAC)-Hg model developed by *Zhang et al*. [2014a, 2014b]. This model has been extensively evaluated with observations for both surface and subsurface ocean waters and has been used to simulate the natural Hg cycle in the ocean and its perturbation by human influence. Here we implement Hg chemistry in the MITgcm to take advantage of the carbon and ecosystem parameters in the DARWIN simulation. Briefly, the model tracks three forms of Hg: dissolved elemental Hg (Hg^0), dissolved divalent Hg (Hg^{II}), and particle-bound Hg (Hg^P). Hg biogeochemistry includes photochemical and biological redox reactions between Hg^0 and Hg^{II} as described in *Soerensen et al*. [2010].

For Hg in seawater, an instantaneous equilibrium is assumed between Hg^{II} and Hg^P based on a specified partition coefficient (K_d) and the POC concentration [*Zhang et al*., 2014a]. Over the Arctic Ocean, we use the K_d from *Fisher et al*. [2012]. Each form of Hg is transported laterally and vertically by oceanic circulation and mixing. Hg^P additionally settles vertically as POC in the oceanic water column. Air-sea exchange of Hg^0 is proportional to the concentration gradient of Hg^0 across the air-sea interface, the open water fraction in sea ice covered areas, and a piston velocity following the parameterization described in *Nightingale et al*. [2000]. Based on the results of *Loose et al*. [2014], we double the piston velocity over regions that are partially covered by sea ice to account for enhanced shear stress and convection-driven turbulence due to ice rafting. Hg inputs from rivers are added to surface ocean grid boxes at river mouths with month-to-month variability proportional to freshwater discharge [*Dai and Trenberth*, 2002].

Dissolved phase Hg from rivers enters the ocean as Hg^{II} complexes. Particulate Hg from rivers is simulated using a separate refractory Hg^P tracer to reflect the strong binding to POC of terrestrial origin. This refractory Hg^P is only released to the dissolved phase when the organic carbon is remineralized. *Loibner et al*. [2006] showed that the release of Hg from terrestrial POC is slowed because of encapsulation in the microporous structure. Leaching experiments find that less than 10% of total Hg in the soil organic carbon is water soluble within the first 24 to 48 h [*G Liu et al*., 2006; *Xu et al*., 2014]. We prescribe a rate of $1\,yr^{-1}$ for the release of refractory Hg^P to the dissolved phase, based on estimates of terrestrial POC remineralization rates in the ocean [*Hansell et al*., 2009; *Hedges et al*., 1997]. Based on prior work, we assume a settling velocity of $3\,m\,d^{-1}$ for refractory Hg^P [*Harris et al*., 2005; *Xu et al*., 2011].

We estimate the burial of riverine Hg in estuarine sediments using the typology system developed by *Walsh and Nittrouer* [2009]. This classification system describes sediment transport and dispersal on continental margins for 23 river systems. Five river types are identified: (1) estuarine accumulation dominated (EAD) where river flow is weak and particle loads are small; (2) proximal accumulation dominated (PAD) where small fractions of sediment are exported to the open ocean; (3) canyon captured (CC) where the majority of river sediment load is rapidly exported to the deep sea via a submarine canyon; (4) marine dispersal dominated (MDD) where most of the sediment load is dispersed on the continental margin; and (5) subaqueous delta clinoform (SDC) where tidal flows carry the sediment load great distances from the shoreline. We use detailed studies of the sediment transport budget of each characteristic river type (Table 1) to assign different fractions of sediment exported (10% to 60%) beyond the estuarine environment.

The behavior and reactivity of Hg associated with POC in freshwater and marine systems plays a major role in determining the fate of river-derived Hg and is not well constrained by observations. We performed two sensitivity simulations to investigate plausible scenarios for Hg chemistry that vary partitioning of Hg^{II} between the dissolved and solid phases. We consider extreme cases to bracket the influence of Hg inputs from rivers on ocean concentrations. "Reversible equilibrium" allows Hg^{II} in rivers and seawater to partition instantaneously with particles in solution based on a specified partition coefficient constrained by observations [*Soerensen et al*., 2010] rather than assuming that the Hg associated with riverine particulate matter is refractory in nature and does not readily desorb ("refractory particles").

The model is forced with external inputs from rivers and atmospheric deposition for the recent decade (2000–2010). Present-day Hg inputs from rivers to different ocean basins are based on *Amos et al*. [2014] with a global total of $27\,Mmol\,yr^{-1}$ Hg^P and $0.87\,Mmol\,yr^{-1}$ in the dissolved phase. Initial Hg

Table 1. Export of Riverine Hg From Estuaries for Different River Types

River Type	f_{export}[a]	Typical Rivers
Estuarine accumulation dominated (EAD)	0.10	Colorado[b] and Susquehanna[c]
Proximal accumulation dominated (PAD)	0.20	Mississippi[d], Rhône[e], Ob[f], Yenisey[f], Yellow[g], and Yukon[h]
Canyon captured (CC)	0.60	Sepik[i] and Congo[j]
Marine dispersal dominated (MDD)	0.60	Eel[k], Columbia[l], and Pearl[g]
Subaqueous delta clinoform (SDC)	0.50	Fly[m], Amazon[n], and Yangtze[g]

[a]Fraction of particulate Hg from rivers transported beyond the estuarine region (the 55 m isodepth).
[b]*Carriquiry and Sánchez* [1999].
[c]*Langland and Cronin* [2000].
[d]*K. Xu et al.* [2011].
[e]*Zuo et al.* [1991].
[f]*Stein et al.* [2004].
[g]*J. Liu et al.* [2009].
[h]*Nelson* [1980].
[i]*Walsh and Nittrouer* [2003].
[j]*Droz et al.* [1996].
[k]*Harris et al.* [2005] and *Sommerfield et al.* [1999].
[l]*Nittrouer et al.* [1979] and *Spahn et al.* [2009].
[m]*Walsh et al.* [2004].
[n]*Kuehl et al.* [1986].

concentrations in the ocean for the base case simulation are from the OFFTRAC model [*Zhang et al.*, 2014b]. Atmospheric Hg deposition at 4° × 5° horizontal resolution and monthly temporal resolution are taken from the GEOS-Chem Hg simulation as described in *Zhang et al.* [2012]. Anthropogenic Hg emissions are from the Global Emission Inventory Activity 2005 inventory (http://www.geiacenter.org). We use monthly evasion fluxes from the MITgcm as a bottom boundary condition for the GEOS-Chem atmospheric Hg simulation to evaluate the contribution of Hg sources from circumpolar rivers to the Arctic atmospheric Hg concentrations.

3. Results and Discussion

3.1. Model Evaluation

Figure 1 compares modeled and observed (2002–2011) total Hg concentrations in surface seawater (0–10 m depth) for both the global and Arctic Ocean simulations. Globally, modeled (mean and standard deviation: 0.63 ± 0.15 pM) and observed (0.86 ± 0.52 pM) seawater concentrations do not differ significantly

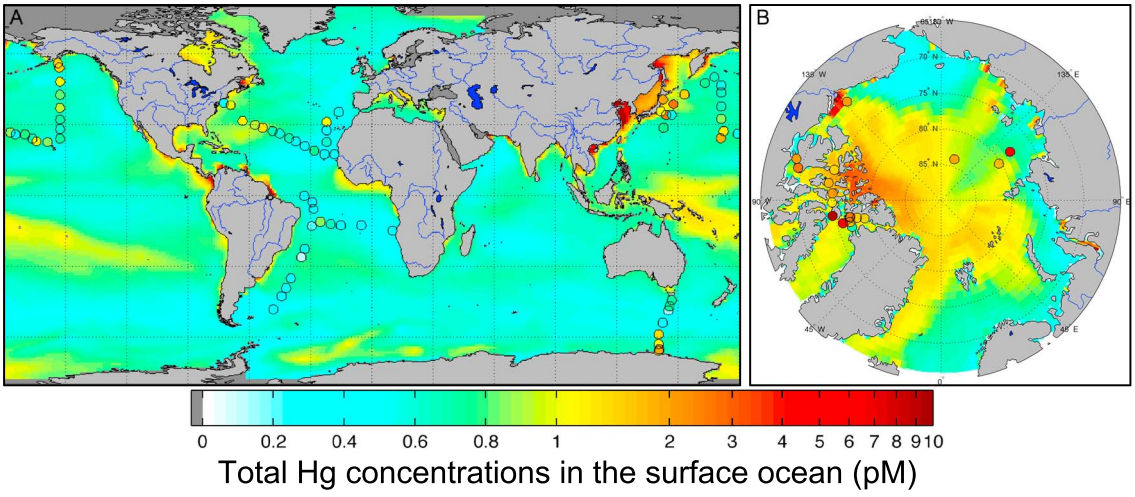

Figure 1. Total Hg concentrations (pM) in the surface ocean (0–10 m depth), (a) globally, and (b) for the Arctic. Model results include inputs from atmospheric deposition and riverine discharge (solid contours) compared to observations from 2002 to 2011 ship cruises (circles). The global model assumes that riverine Hg^P is refractory, while the Hg^P from Arctic rivers is allowed to freely desorb. The model values are the annual mean of total Hg concentrations. Observations are from the North Pacific Ocean [*Laurier et al.*, 2004; *Sunderland et al.*, 2009], the North Atlantic Ocean [*Bowman et al.*, 2014], the South Atlantic Ocean [*Bowman et al.*, 2012], the Southern Ocean [*Cossa et al.*, 2011], and the Arctic Ocean [*Kirk et al.*, 2008; *Lehnherr et al.*, 2011; *Heimbürger et al.*, 2015].

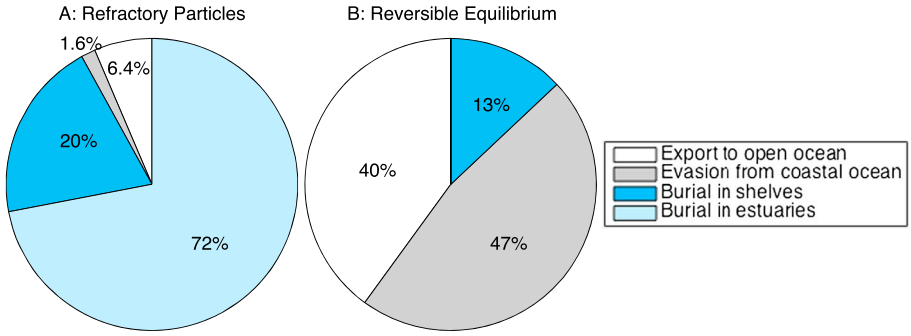

Figure 2. Results of sensitivity simulations contrasting the global fate of Hg discharged by rivers. (a) Results of simulations when particles are specified as refractory in nature (Hg^{II} does not readily desorb). (b) Results of the "reversible equilibrium" scenario where particulate phase Hg is allowed to readily sorb and desorb. Estuaries, shelves, and open ocean are defined as ocean regions with depth $<$ 55 m, 55–185 m, and $>$185 m, respectively. Coastal ocean refers to estuaries and the shelf.

(t test, $p > 0.05$) (Figure 1a). The model reproduces observed spatial patterns such as enhanced concentrations off the coast of East Asia and eastern North America. It also reproduces lower observed Hg concentrations in regions with reduced atmospheric inputs such as the eastern North Atlantic Ocean, the central North Pacific Ocean, and the northern portion of the Southern Ocean. Both the model and observations indicate enhanced Hg concentrations in the south Southern Ocean, reflecting the upwelling of deeper waters that are higher in Hg due to particle scavenging [*Cossa et al*., 2011; *Zhang et al*., 2014b].

Figure 1b shows that modeled (1.2 ± 0.3 pM) and observed (1.6 ± 0.5 pM) surface seawater concentrations in the Arctic Ocean do not differ significantly ($p > 0.05$). Our simulation is consistent with available observations showing that the Arctic Ocean is enriched in total Hg relative to the lower latitudes due to inputs from rivers and springtime mercury depletion events (MDEs) and reduced evasion losses due to sea ice cover [*Andersson et al*., 2008]. The western Arctic Ocean displays higher concentrations than the eastern Arctic due to more frequent MDEs [*Kirk et al*., 2012] and greater summertime ice cover (Figure 1B).

3.2. Relative Reactivity of Riverine and Atmospheric Hg Pools

The amount of riverine Hg that settles in estuaries and on the shelf is highly sensitive to the fraction of the Hg^P pool specified as refractory. Figure 2 contrasts two different scenarios for the fate of Hg discharges from rivers. The first considers all the Hg^P to be refractory (Hg attached to particles does not desorb), while the second allows continuous reequilibration between the dissolved and solid phases based on the concentration of suspended particulate matter in solution (reversible equilibrium). When the Hg from rivers is specified as refractory, 72% is buried in estuarine sediments (ocean depth $<$ 55 m) based on the classification scheme described in Table 1. For the remaining fraction, 20% is sequestered in shelf sediments (55 m $<$ ocean depth $<$ 185 m), 1.6% is evaded to the atmosphere in the estuarine and shelf regions, and 6.4% is transported to the open ocean (ocean depth $>$ 185 m). In the reversible equilibrium simulation, most of the riverine Hg is evaded to the atmosphere in the estuarine and shelf regions (47%) and open ocean (40%) rather than being buried in shelf sediments (13%).

The actual fate of Hg^P discharges from rivers lies between these two extremes depending on the size of the refractory POC pool [*Blair and Aller*, 2012]. Many rivers in the middle and low latitudes exhibit enhanced mechanical weathering and high refractory POC loads, especially on the Pacific Rim [*Milliman and Syvitski*, 1992]. In the reversible equilibrium simulation, the total global evasion flux (36 Mmol yr^{-1}) exceeds the confidence limits reported by *Sunderland and Mason* [2007] (9.7–21 Mmol yr^{-1} as 90% confidence interval) from a synthesis of observations. Simulated Hg concentrations in seawater are also much higher than observations (Figure S1 in the supporting information). We therefore infer that most of the Hg^P in middle- and low-latitude rivers is refractory. Recent measurements show similar or lower evasion rates from coastal than open ocean [*Ci et al*., 2014; *Soerensen et al*., 2013; *Tseng et al*., 2013]. These results imply that atmospherically deposited Hg to the open ocean in the middle and lower latitudes is more accessible for methylation and biological uptake than inputs from rivers, as suggested by recent work [*Jonsson et al*., 2014].

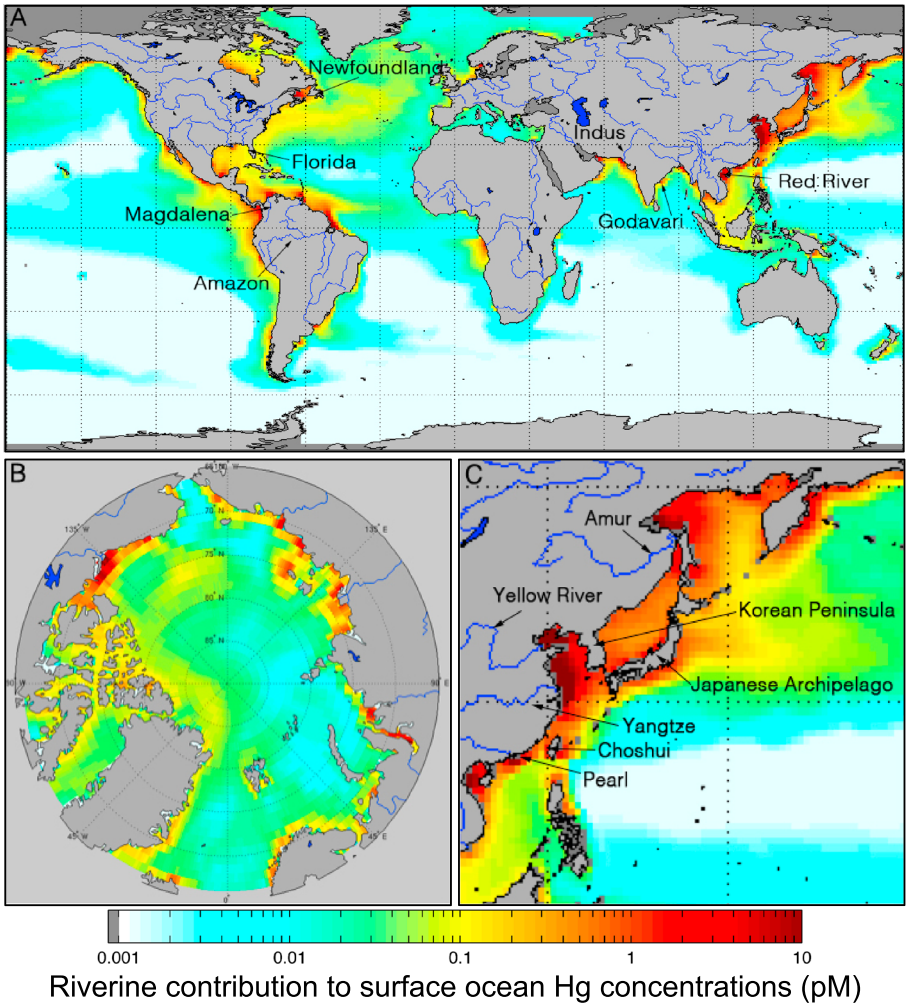

Figure 3. Contributions of riverine discharges to modeled annual total Hg concentrations (pM) at 0–10 m depth. (a) Global ocean simulation, (b) Arctic Ocean simulation, and (c) zoom for the western Pacific Rim.

By contrast, results of the reversible equilibrium simulation for the Arctic Ocean are consistent with available total Hg concentrations measured in surface seawater (Figure 1B). This can be explained in part by suspended particulate loads in Arctic rivers that are approximately an order of magnitude lower than the global mean due to thin weathering crusts and low precipitation and temperature in their watersheds [*Gordeev*, 2006].

3.3. Spatial Heterogeneity in River Influences Across Ocean Regions

Figure 3 shows that the spatial influence of many rivers is limited to ocean margins. Globally, Hg discharges from rivers account for only 4% (0.022 pM) of the measured total concentrations in surface seawater. The world's largest three rivers (Yellow, Yangtze, and Amazon) account for 40% of freshwater Hg discharges to the coastal ocean but do not substantially impact Hg concentrations in surface seawater beyond the shelf. The Yellow and Yangtze Rivers deliver only 2.6% of their total Hg load (9.4 Mmol yr^{-1}) to the open ocean because the Korean Peninsula and Japanese archipelago provide physical barriers to particulate Hg transport and retain Hg near ocean margins. Similarly, physical barriers imposed by surrounding landmasses limit offshore transport of Hg from the Red, Amur, Choshui, and Magdalena Rivers (Figure 3). The Amazon River is the largest exporter of freshwater and particulate matter to marine waters globally (Table 2), but Hg discharges are transported northwestward along the Brazilian continental shelf, with no significant offshore transport until they intersect the Equatorial Counter Current around 7°N (Figure 3). This is consistent with the apparent absence of a riverine Hg plume and low total Hg concentrations (0.8–1.7 pM) observed in the open Equatorial Atlantic Ocean near the Amazon River mouth [*Mason and Sullivan*, 1999].

Table 2. Ten Largest Rivers Globally Ranked by Hg Discharges to Ocean Margins[a]

River	River Discharge		Hg Discharge (Mmol yr^{-1})	Fraction in Dissolved Phase(%)	Type as Defined in Table 1
	Water (km^3 yr^{-1})	TSS[b] (Tg yr^{-1})			
Yellow	47 ± 14	1100 ± 840	6.5 ± 8.3	0.078	PAD
Yangtze	910 ± 130	480 ± 180	2.9 ± 2.7	3.4	SDC
Amazon	5300 ± 430	1200 ± 380	2.0 ± 1.6	7.7	SDC
Red	36 ± 12	130 ± 62	0.77 ± 0.79	0.52	SDC
Indus	100 ± 25	250 ± 120	0.68 ± 0.69	0.72	PAD
Godavari	97 ± 32	170 ± 120	0.46 ± 0.56	1.0	CC
Pearl	340 ± 47	69 ± 26	0.44 ± 0.39	7.4	MDD
Choshui	5.2 ± 1.1	63 ± 13	0.37 ± 0.32	0.15	MDD
Magdalena	230 ± 35	220 ± 82	0.33 ± 0.31	1.9	CC
Amur	310 ± 60	52 ± 6.6	0.34 ± 0.26	11	PAD
Global	37,000	16,000	28 ± 13	3.1	

[a]Adapted from *Amos et al.* [2014]. Values represent present-day annual means and standard errors. Fresh water discharge is from *Dai and Trenberth* [2002] and references therein.
[b]TSS = total suspended solids, data from *Ludwig et al.* [2011] and references therein.

Physical retention of particulate Hg loads in nearshore regions has a major impact on contamination of coastal and shelf regions. Our modeling results suggest that rivers contribute more than 90% of the Hg to inland seas (Bohai Bay and the adjacent Yellow Sea) that have a simulated mean concentration in seawater of 10 ± 7.6 pM. High modeled Hg concentrations agree with elevated Hg (8.4 ± 1.7 pM) and low salinity (<33 practical salinity units) observed in seawater from this region [*Ci et al.*, 2011].

Oceanic impacts of Hg discharged by several smaller rivers are enhanced by major currents such as the Gulf Stream in the North Atlantic and the Kuroshio in the North Pacific (Figure 3). Our results show that the largest proportion of Hg from rivers transported to the open ocean (25% of total load) is from several smaller rivers along the eastern coastline of North America. Freshwater discharges are transported offshore and eventually are entrained into the Gulf Stream. Current velocities within the Gulf Stream reach 1–2 m s^{-1} and can thus transport Hg from rivers across the North Atlantic Ocean in several weeks. Surface ocean Hg concentrations near the Gulf Stream are elevated by 0.05–0.1 pM, and the riverine signal is still distinguishable in the eastern North Atlantic near Europe (Figure 3a). Figure 3 similarly shows a plume of Hg across the Western North Pacific carried by Kuroshio extension that originates from the relatively smaller Japanese and Russian rivers rather than the most polluted Chinese rivers.

3.4. Fate of Hg From Arctic Rivers

Biogeochemical processes affecting the fate of Hg discharged by rivers in the Arctic Ocean differ from the middle and low latitudes. As discussed above, the refractory component of the Hg load from Arctic rivers is substantially smaller than other regions due to lower particulate loads [*Bouchez et al.*, 2010; *Gordeev*, 2006]. Microbial communities in Arctic river deltas have adapted to strong seasonal variability in temperature, ice cover, nutrient availability, light, and salinity. Prior work suggests that these adaptations allow more efficient metabolism of POC by Arctic microbial communities compared to middle and low latitudes [*Bianchi*, 2011; *Macdonald et al.*, 2005; *Rontani et al.*, 2014].

Our modeling results (Figure 3b) suggest that riverine Hg preferentially enhances surface ocean concentrations in the nearshore regions of the Arctic, which is consistent with observations of elevated concentrations near river mouths in the Arctic [*Andersson et al.*, 2008; *Wang et al.*, 2012]. Sea ice melt in estuaries is accelerated by heat transferred from freshwater discharge during seasonal snowmelt in May and June [*Nghiem et al.*, 2014]. This increases the transfer velocity of Hg^0, and therefore Hg^0 evasion, by enhancing turbulence of surface waters due to mechanical shear associated with drifting ice and buoyant convection during ice melting [*Loose et al.*, 2014]. Model results show that melting sea ice also enhances Hg^0 evasion near river mouths by increasing the surface area of seawater in direct contact with the atmosphere. These results corroborate the findings of *Sommar et al.* [2010] showing enhanced Hg^0 evasion and elevated atmospheric concentrations near the Mackenzie River. Conversely, *Fisher et al.* [2012] assume that the Hg from rivers is uniformly distributed in the entire Arctic Ocean, including the high Arctic, where the transfer velocity of Hg^0 is low because of the presence of perennial sea ice.

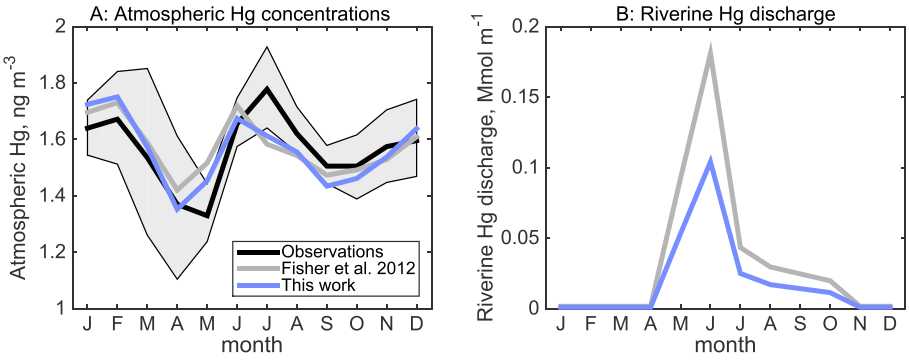

Figure 4. Atmospheric and riverine mercury in the Arctic. (a) Mean seasonal variation of modeled and observed atmospheric mercury concentrations. (b) Seasonal Hg discharges from Arctic rivers used to force model simulation. Figure 4a averages observations and model values for Alert, Canada (83°N, 62°W) [*Steffen et al*., 2005], Zeppelin Mountain, Norway (79°N, 12°E) [*Berg et al*., 2008], and Amderma, Russia (70°N, 62°E) [*Steffen et al*., 2005]. Model values from this work (purple) are compared to the previous model study from *Fisher et al*. [2012]. Grey shading indicates the standard deviation of the observations among sites. Figure 4b contrasts inferred riverine Hg discharges required to explain the observed summer rebound in Arctic atmospheric Hg concentrations in this work (purple line) with prior estimates (green line) using the GEOS-Chem model [*Fisher et al*., 2012].

Overall, we find that a greater portion of riverine Hg in the Arctic is subject to evasion (80%) than in the study of *Fisher et al*. [2012] (54%).

Observed atmospheric mercury concentrations reach minimum levels in the Arctic springtime but rebound to peak levels between June and August (Figure 4a). *Fisher et al*. [2012] showed that enhanced oceanic evasion during those months could explain this summer rebound in atmospheric Hg concentrations and hypothesized that Hg inputs (0.47 Mmol yr^{-1}) from rivers and coastal erosion were the most likely sources. In our Arctic Ocean simulation, substantially lower Hg inputs (0.31 Mmol Hg yr^{-1}) are needed to sustain observed atmospheric Hg concentrations. The spatial pattern of evasion in our model is concentrated near river mouths, but this could still enhance atmospheric concentrations at distant observational sites because Hg^0 is quickly transported throughout the Arctic atmosphere (Figure 4a).

Smaller Hg loading to the marginal Arctic Ocean is needed to force the summer rebound in atmospheric Hg concentrations in our simulation than what is suggested by *Fisher et al*. [2012]. The source from coastal erosion is estimated to be 0.08 Mmol yr^{-1} [*Rachold et al*., 2004], which implies a contribution from rivers of 0.23 Mmol yr^{-1}. This is within the range of riverine inputs from *Dastoor and Durnford* [2014] (0.25 Mmol yr^{-1}) based on Hg:DOC ratios and close to the upper estimate based on direct Hg measurements (0.22 Mmol yr^{-1}) by *Amos et al*. [2014]. It is approximately half of the magnitude proposed by *Fisher et al*. [2012] (0.40 Mmol yr^{-1}) (Figure 4b). Even with this lower discharge, we find that Hg inputs to the Arctic Ocean from rivers provide a plausible explanation for the observed summer peak in the Arctic atmosphere and are similar in magnitude to atmospheric inputs [*Kirk et al*., 2012].

4. Summary and Conclusions

We have developed a new capability for global 3-D modeling of oceanic Hg coupled to plankton dynamics and carbon respiration and applied it to better understand the global influence of riverine Hg on different marine regions. This involved a classification scheme for particle transport from different river types to estimate the fraction of the suspended solid load transported beyond the estuarine region, which varies from 10% to 60%.

Our results show that the amount of Hg discharged from rivers that settles in estuaries and on the shelf is highly sensitive to the fraction of the particulate Hg pool that is refractory in nature. Observational constraints on seawater Hg concentrations and air-sea exchange suggest that most Hg from rivers in the global ocean is refractory. A notable exception appears to be the Arctic region, where the low particle load and the efficient degradation of particulate organic carbon favor a more labile riverine Hg pool. On a global basis, 20 Mmol yr^{-1} (72%) of the Hg inputs from rivers are buried in estuarine sediments, 5.5 Mmol (20%) is scavenged by suspended sediments and buried in shelf sediments, 0.45 Mmol (1.6%) is evaded to the atmosphere from coastal regions, and 1.8 Mmol (6.4%) is transported to the open ocean.

Our modeling results show strong regional variability in the transport of Hg discharged by rivers to the open ocean. Only a small fraction of large Hg discharges (2.6%) from the Yellow and Yangtze Rivers is transported beyond the shelf due to physical barriers imposed by the Korean Peninsula and Japanese archipelago. Riverine Hg discharges from the Amazon are diverted northwestward along the Brazilian continental shelf and attenuated before converging with a major ocean current, thus minimally affecting oceanic Hg concentrations. Conversely, rivers from the east coast of North America deliver up to 25% of their total load to the North Atlantic facilitated by the Gulf Stream.

Our results suggest that riverine Hg dynamics in the Arctic differ substantially from the middle and low latitudes. We find that enhanced turbulence associated with sea ice dynamics facilitates increased evasion of Hg discharged by Arctic rivers in estuaries. Model results suggest that rivers contribute substantially to Arctic atmospheric Hg contributions. Based on improved ocean circulation, biogeochemistry, and sea ice dynamics, we infer that a total Hg load of 0.31 Mmol yr^{-1} (0.08 Mmol yr^{-1} coastal erosion and 0.23 Mmol yr^{-1} rivers) is required to reproduce the observed summer maximum in atmospheric concentrations. This is within the range of recent estimates of total Hg discharges from Arctic rivers. Our results imply that rivers are a plausible explanation for the observed summer peak in the Arctic atmosphere and are similar in magnitude to atmospheric inputs.

Acknowledgments
We acknowledge financial support for this work from the U.S. National Science Foundation (grants: PLR: 1023213 and 1260464 and OCE: 1130549) and the Electric Power Research Institute (EPRI). We thank Dimitris Menemenlis at MIT for their assistance with the Arctic configuration of the MITgcm used in this study. All the data sets and models used in this paper are available on our group website (http://bgc.seas.harvard.edu).

References

Amos, H. M., D. J. Jacob, D. Kocman, H. M. Horowitz, Y. Zhang, S. Dutkiewicz, M. Horvat, E. S. Corbitt, D. P. Krabbenhoft, and E. M. Sunderland (2014), Global biogeochemical implications of mercury discharges from rivers and sediment burial, *Environ. Sci. Technol.*, *48*(16), 9514–9522.

Andersson, M. E., J. Sommar, K. Gårdfeldt, and O. Lindqvist (2008), Enhanced concentrations of dissolved gaseous mercury in the surface waters of the Arctic Ocean, *Mar. Chem.*, *110*(3–4), 190–194.

Berg, T., K. Aspmo, and E. Steinnes (2008), Transport of Hg from atmospheric mercury depletion events to the mainland of Norway and its possible influence on Hg deposition, *Geophys. Res. Lett.*, *35*, L09802, doi:10.1029/02008GL033586.

Bianchi, T. S. (2011), The role of terrestrially derived organic carbon in the coastal ocean: A changing paradigm and the priming effect, *Proc. Natl. Acad. Sci. U.S.A.*, *108*(49), 19,473–19,481.

Blair, N. E., and R. C. Aller (2012), The fate of terrestrial organic carbon in the marine environment, *Annu. Rev. Mar. Sci.*, *4*, 401–423.

Bouchez, J., O. Beyssac, V. Galy, J. Gaillardet, C. France-Lanord, L. Maurice, and P. Moreira-Turcq (2010), Oxidation of petrogenic organic carbon in the Amazon floodplain as a source of atmospheric CO_2, *Geology*, *38*(3), 255–258.

Bowman, K. L., T. J. Kading, G. Swarr, C. Hammerschmidt, C. Lamborg, and M. J. A. Rijkenberg (2012), Mercury species and thiols from GEOTRACES cruises in the North and South Atlantic Ocean, *Mineralog. Mag.*, 76, 1504.

Bowman, K. L., C. R. Hammerschmidt, C. H. Lamborg, and G. Swarr (2014), Mercury in the North Atlantic Ocean: The US GEOTRACES zonal and meridional sections, *Deep Sea Res., Part II*, doi:10.1016/j.dsr1012.2014.1007.1004.

Carriquiry, J. D., and A. Sánchez (1999), Sedimentation in the Colorado River delta and Upper Gulf of California after nearly a century of discharge loss, *Mar. Geol.*, *158*(1), 125–145.

Chester, R. (2003), The transport of material to the oceans: Relative flux magnitudes, in *Marine Geochemistry*, edited by R. Chester, pp. 98–134, Blackwell Science, Oxford, U. K.

Ci, Z., X. S. Zhang, Z. W. Wang, Z. C. Niu, X. Y. Diao, and S. W. Wang (2011), Distribution and air-sea exchange of mercury (Hg) in the Yellow Sea, *Atmos. Chem. Phys.*, *11*(6), 2881–2892.

Ci, Z., C. Wang, Z. Wang, and X. Zhang (2014), Elemental mercury (Hg(0)) in air and surface waters of the Yellow Sea during late spring and late fall 2012: Concentration, spatial-temporal distribution and air/sea flux, *Chemosphere*, *119C*, 199–208.

Cossa, D., L.-E. Heimbürger, D. Lannuzel, S. R. Rintoul, E. C. V. Butler, A. R. Bowie, B. Averty, R. J. Watson, and T. Remenyi (2011), Mercury in the Southern Ocean, *Geochim. Cosmochim. Acta*, *75*(14), 4037–4052.

Dai, A., and K. E. Trenberth (2002), Estimates of freshwater discharge from continents: Latitudinal and seasonal variations, *J. Hydrometeorol.*, *3*, 660–687.

Dastoor, A. P., and D. A. Durnford (2014), Arctic Ocean: Is it a sink or a source of atmospheric mercury?, *Environ. Sci. Technol.*, *48*(3), 1707–1717.

Droz, L., F. Rigaut, P. Cochonat, and R. Tofani (1996), Morphology and recent evolution of the Zaire turbidite system (Gulf of Guinea), *Geol. Soc. Am. Bull.*, *108*(3), 253–269.

Dutkiewicz, S., B. A. Ward, F. Monteiro, and M. J. Follows (2012), Interconnection of nitrogen fixers and iron in the Pacific Ocean: Theory and numerical simulations, *Global Biogeochem. Cycles*, *26*, GB1012, doi:10.1029/2011GB004039.

Emmerton, C. A., J. A. Graydon, J. A. Gareis, V. L. S. Louis, L. F. Lesack, J. K. Banack, F. Hicks, and J. Nafziger (2013), Mercury export to the Arctic Ocean from the Mackenzie River, Canada, *Environ. Sci. Technol.*, *47*(14), 7644–7654.

Fisher, J. A., D. J. Jacob, A. L. Soerensen, H. M. Amos, A. Steffen, and E. M. Sunderland (2012), Riverine source of Arctic Ocean mercury inferred from atmospheric observations, *Nat. Geosci.*, *5*(7), 499–504.

Gordeev, V. V. (2006), Fluvial sediment flux to the Arctic Ocean, *Geomorphology*, *80*(1–2), 94–104.

Hansell, D. A., C. A. Carlson, D. J. Repeta, and R. Schlitzer (2009), Dissolved organic matter in the ocean: A controversy stimulates new insights, *Oceanography*, *22*(4), 202–211.

Harris, C. K., P. A. Traykovski, and W. R. Geyer (2005), Flood dispersal and deposition by near-bed gravitational sediment flows and oceanographic transport: A numerical modeling study of the Eel River shelf, northern California, *J. Geophys. Res.*, *110*, C09025, doi:10.1029/02004JC002727.

Hedges, J. I., R. G. Keil, and R. Benner (1997), What happens to terrestrial organic matter in the ocean?, *Org. Geochem.*, *27*(5–6), 195–212.

Heimbach, P., D. Menemenlis, M. Losch, J.-M. Campin, and C. Hill (2010), On the formulation of sea-ice models. Part 2: Lessons from multi-year adjoint sea-ice export sensitivities through the Canadian Arctic Archipelago, *Ocean Model.*, *33*(1), 145–158.

Heimburger, L. E., J. E. Sonke, D. Cossa, D. Point, C. Lagane, L. Laffont, B. T. Galfond, M. Nicolaus, B. Rabe, and M. R. van der Loeff (2015), Shallow methylmercury production in the marginal sea ice zone of the central Arctic Ocean, *Scientific Rep.*, *5*, 10318.

Hintelmann, H., R. Harris, A. Heyes, J. P. Hurley, C. A. Kelly, D. P. Krabbenhoft, S. Lindberg, J. W. M. Rudd, K. J. Scott, and V. L. S. Louis (2002), Reactivity and mobility of new and old mercury deposition in a boreal forest ecosystem during the first year of the METAALICUS study, *Environ. Sci. Technol.*, *36*(23), 5034–5040.

Hsu-Kim, H., K. H. Kucharzyk, T. Zhang, and M. A. Deshusses (2013), Mechanisms regulating mercury bioavailability for methylating microorganisms in the aquatic environment: A critical review, *Environ. Sci. Technol.*, *47*(6), 2441–2456.

Jonsson, S., U. Skyllberg, M. B. Nilsson, E. Lundberg, A. Andersson, and E. Bjorn (2014), Differentiated availability of geochemical mercury pools controls methylmercury levels in estuarine sediment and biota, *Nat. Commun.*, *5*, doi:10.1038/ncomms5624.

Kalnay, E., et al. (1996), The NCEP/NCAR 40-year reanalysis project, *Bull. Am. Meteorol. Soc.*, *77*(3), 437–471.

Kirk, J. L., V. L. S. Louis, H. Hintelmann, I. Lehnherr, B. Else, and L. Poissant (2008), Methylated mercury species in marine waters of the Canadian high and sub Arctic, *Environ. Sci. Technol.*, *42*(22), 8367–8373.

Kirk, J. L., et al. (2012), Mercury in arctic marine ecosystems: Sources, pathways and exposure, *Environ. Res.*, *119*, 64–87.

Kuehl, S. A., D. J. DeMaster, and C. A. Nittrouer (1986), Nature of sediment accumulation on the Amazon continental shelf, *Cont. Shelf Res.*, *6*(1), 209–225.

Langland, M., and T. Cronin (2000), A summary report of sediment processes in Chesapeake Bay and Watershed, *USGS Water Resources Investigations Rep. 03–4123*, 122 pp.

Laurier, F. J. G., R. P. Mason, G. A. Gill, and L. Whalin (2004), Mercury distributions in the North Pacific Ocean—20 years of observations, *Mar. Chem.*, *90*(1–4), 3–19.

Lehnherr, I., V. L. S. Louis, H. Hintelmann, and J. L. Kirk (2011), Methylation of inorganic mercury in polar marine waters, *Nat. Geosci.*, *4*, 298–302.

Liu, G., J. Cabrera, M. Allen, and Y. Cai (2006), Mercury characterization in a soil sample collected nearby the DOE Oak Ridge Reservation utilizing sequential extraction and thermal desorption method, *Sci. Total Environ.*, *369*(1), 384–392.

Liu, J., Z. Xue, K. Ross, H. J. Wang, Z. S. Yang, A. C. Li, and S. Gao (2009), Fate of sediments delivered to the sea by Asian large rivers: Long-distance transport and formation of remote alongshore clinothems, *Sediment. Rec.*, *7*(4), 4–9.

Loibner, A., J. Jensen, T. Ter Laak, R. Celis, and T. Hartnik (2006), Sorption and ageing of soil contamination, in *Ecological Risk Assessment of Contaminated Land—Decision Support for Site Specific Investigations*, edited by M. Jensen and M. Mesman, pp. 19–29, EU Project LIBERATION, RIVM Report No. 711701047.

Loose, B., W. R. McGillis, D. Perovich, C. J. Zappa, and P. Schlosser (2014), A parameter model of gas exchange for the seasonal sea ice zone, *Ocean Sci.*, *10*(1), 17–28.

Losch, M., D. Menemenlis, J.-M. Campin, P. Heimbach, and C. Hill (2010), On the formulation of sea-ice models. Part 1: Effects of different solver implementations and parameterizations, *Ocean Model.*, *33*(1), 129–144.

Ludwig, W., P. Amiotte-Suchet, J. L. Probst, F. G. Hall, G. Collatz, B. Meeson, S. Los, E. Brown de Colstoun, and D. Landis (2011), ISLSCP II global river fluxes of carbon and sediments to the oceans, *ISLSCP Initiative II Collection*.

Macdonald, R. W., T. Harner, and J. Fyfe (2005), Recent climate change in the Arctic and its impact on contaminant pathways and interpretation of temporal trend data, *Sci. Total Environ.*, *342*(1–3), 5–86.

Manizza, M., M. J. Follows, S. Dutkiewicz, J. W. McClelland, D. Menemenlis, C. N. Hill, A. Townsend-Small, and B. J. Peterson (2009), Modeling transport and fate of riverine dissolved organic carbon in the Arctic Ocean, *Global Biogeochem. Cycles*, *23*, GB4006, doi:10.1029/2008GB003396.

Marshall, J., C. Hill, L. Perelman, and A. Adcroft (1997), Hydrostatic, quasi-hydrostatic, and nonhydrostatic ocean modeling, *J. Geophys. Res.*, *102*(C3), 5733–5752, doi:10.1029/96JC02776.

Mason, R. P., and K. A. Sullivan (1999), The distribution and speciation of mercury in the South and equatorial Atlantic, *Deep Sea Res., Part II*, *46*(5), 937–956.

Mayorga, E., S. P. Seitzinger, J. A. Harrison, E. Dumont, A. H. W. Beusen, A. F. Bouwman, B. M. Fekete, C. Kroeze, and G. Van Drecht (2010), Global Nutrient Export from WaterSheds 2 (NEWS 2): Model development and implementation, *Environ. Modell. Softw.*, *25*(7), 837–853.

Menemenlis, D., C. Hill, A. Adcrocft, J. M. Campin, B. Cheng, B. Ciotti, I. Fukumori, P. Heimbach, C. Henze, and A. Köhl (2005), NASA supercomputer improves prospects for ocean climate research, *Eos Trans. AGU*, *86*(9), 89–96.

Milliman, J. D., and J. P. M. Syvitski (1992), Geomorphic/tectonic control of sediment discharge to the ocean: The importance of small mountainous rivers, *J. Geol.*, *100*, 525–544.

Morel, F. M. M., A. M. L. Kraepiel, and M. Amyot (1998), The chemical cycle and bioaccumulation of mercury, *Annu. Rev. Ecol. Syst.*, *29*, 543–566.

Nelson, C. H. (1980), Graded storm sand layers offshore from the Yukon delta, Alaska, in *Geological, Geochemical and Geotechnical Observations of the Bering Shelf, Alaska*, edited by M. C. Larsen, C. H. Nelson, and D. R. Thor, pp. 80–979, U.S. Geol. Surv., Menlo Park, Calif.

Nghiem, S. V., D. K. Hall, I. G. Rigor, P. Li, and G. Neumann (2014), Effects of Mackenzie River discharge and bathymetry on sea ice in the Beaufort Sea, *Geophys. Res. Lett.*, *41*, 873–879, doi:10.1002/2013GL058956.

Nightingale, P. D., G. Malin, C. S. Law, A. J. Watson, P. S. Liss, M. I. Liddicoat, J. Boutin, and R. C. Upstill-Goddard (2000), In situ evaluation of air-sea gas exchange parameterizations using novel conservative and volatile tracers, *Global Biogeochem. Cycles*, *14*(1), 373–387, doi:10.1029/1999GB900091.

Nittrouer, C. A., R. W. Sternberg, R. Carpenter, and J. T. Bennett (1979), The use of Pb-210 geochronology as a sedimentological tool: Application to the Washington continental shelf, *Mar. Geol.*, *31*(3), 297–316.

Opsahl, S., R. Benner, and R. M. W. Amon (1999), Major flux of terrigenous dissolved organic matter through the Arctic Ocean, *Limnol. Oceanogr.*, *44*(8), 2017–2023.

Oswald, C. J., A. Heyes, and B. A. Branfireun (2014), Fate and transport of ambient mercury and applied mercury isotope in terrestrial upland soils: Insights from the METAALICUS watershed, *Environ. Sci. Technol.*, *48*(2), 1023–1031.

Rachold, V., H. Eicken, V. V. Gordeev, M. N. Grigoriev, H.-W. Hubberten, and A. P. Lisitzin (2004), Modern terrigenous organic carbon input to the Arctic Ocean, in *The Organic Carbon Cycle in the Arctic Ocean*, edited by R. Stein et al., pp. 33–55, Springer, Berlin.

Ravichandran, M. (2004), Interactions between mercury and dissolved organic matter—A review, *Chemosphere*, *55*(3), 319–331.

Rontani, J.-F., B. Charrière, R. Sempéré, D. Doxaran, F. Vaultier, J. E. Vonk, and J. K. Volkman (2014), Degradation of sterols and terrigenous organic matter in waters of the Mackenzie Shelf Canadian Arctic, *Org. Geochem.*, *75*, 61–73.

Schuster, P. F., R. G. Striegl, G. R. Aiken, D. P. Krabbenhoft, J. F. Dewild, K. Butler, B. Kamark, and M. Dornblaser (2011), Mercury export from the Yukon River Basin and potential response to a changing climate, *Environ. Sci. Technol.*, *45*(21), 9262–9267.

Soerensen, A. L., E. M. Sunderland, C. D. Holmes, D. J. Jacob, R. M. Yantosca, H. Skov, J. H. Christensen, S. A. Strode, and R. P. Mason (2010), An improved global model for air-sea exchange of mercury: High concentrations over the North Atlantic, *Environ. Sci. Technol.*, *44*(22), 8574–8580.

Soerensen, A. L., R. P. Mason, P. H. Balcom, and E. M. Sunderland (2013), Drivers of surface ocean mercury concentrations and air-sea exchange in the West Atlantic Ocean, *Environ. Sci. Technol.*, *47*(14), 7757–7765.

Sommar, J., M. E. Andersson, and H. W. Jacobi (2010), Circumpolar measurements of speciated mercury, ozone and carbon monoxide in the boundary layer of the Arctic Ocean, *Atmos. Chem. Phys.*, *10*(11), 5031–5045.
Sommerfield, C. K., C. A. Nittrouer, and C. R. Alexander (1999), 7Be as a tracer of flood sedimentation on the Northern California continental margin, *Cont. Shelf Res.*, *19*(3), 335–361.
Spahn, E. Y., A. R. Horner-Devine, J. D. Nash, D. A. Jay, and L. Kilcher (2009), Particle resuspension in the Columbia River plume near field, *J. Geophys. Res.*, *114*, C00B14, doi:10.1029/2008JC004986.
Steffen, A., W. Schroeder, R. Macdonald, L. Poissant, and A. Konoplev (2005), Mercury in the Arctic atmosphere: An analysis of eight years of measurements of GEM at Alert (Canada) and a comparison with observations at Amderma (Russia) and Kuujjuarapik (Canada), *Sci. Total Environ.*, *342*(1), 185–198.
Stein, R., et al. (2004), Arctic (palaeo) river discharge and environmental change: Evidence from the Holocene Kara Sea sedimentary record, *Quat. Sci. Rev.*, *23*(11–13), 1485–1511.
Stow, J., E. Krummel, T. Leech, and S. Donaldson (2011), What is the impact of mercury contamination on human health in the Arctic? in *AMAP Assessment 2011: Mercury in the Arctic*, edited by AMAP, pp. 159–170, Arctic Monitoring and Assessment Programme, Oslo.
Sunderland, E. M. (2007), Mercury exposure from domestic and imported estuarine and marine fish in the U.S. seafood market, *Environ. Health Perspect.*, *115*(2), 235–242.
Sunderland, E. M., and R. P. Mason (2007), Human impacts on open ocean mercury concentrations, *Global Biogeochem. Cycles*, *21*, GB4022, doi:10.1029/2006GB002876.
Sunderland, E. M., D. P. Krabbenhoft, J. W. Moreau, S. A. Strode, and W. M. Landing (2009), Mercury sources, distribution, and bioavailability in the North Pacific Ocean: Insights from data and models, *Global Biogeochem. Cycles*, *23*, GB2010, doi:10.1029/2008GB003425.
Tseng, C. M., C. H. Lamborg, and S. C. Hsu (2013), A unique seasonal pattern in dissolved elemental mercury in the South China Sea, a tropical and monsoon-dominated marginal sea, *Geophys. Res. Lett.*, *40*, 167–172, doi:10.1029/2012GL054457.
Walsh, J. P., and C. A. Nittrouer (2003), Contrasting styles of off-shelf sediment accumulation in New Guinea, *Mar. Geol.*, *196*(3–4), 105–125.
Walsh, J. P., and C. A. Nittrouer (2009), Understanding fine-grained river-sediment dispersal on continental margins, *Mar. Geol.*, *263*(1–4), 34–45.
Walsh, J. P., C. A. Nittrouer, C. M. Palinkas, A. S. Ogston, R. W. Sternberg, and G. J. Brunskill (2004), Clinoform mechanics in the Gulf of Papua, New Guinea, *Cont. Shelf Res.*, *24*(19), 2487–2510.
Wang, F., R. W. Macdonald, D. A. Armstrong, and G. A. Stern (2012), Total and methylated mercury in the Beaufort Sea: The role of local and recent organic remineralization, *Environ. Sci. Technol.*, *46*(21), 11,821–11,828.
Whalin, L., E.-H. Kim, and R. Mason (2007), Factors influencing the oxidation, reduction, methylation and demethylation of mercury species in coastal waters, *Mar. Chem.*, *107*(3), 278–294.
Wunsch, C., and P. Heimbach (2007), Practical global oceanic state estimation, *Phys. D (Amsterdam, Neth.)*, *230*(1), 197–208.
Xu, J., D. B. Kleja, H. Biester, A. Lagerkvist, and J. Kumpiene (2014), Influence of particle size distribution, organic carbon, pH and chlorides on washing of mercury contaminated soil, *Chemosphere*, *109*, 99–105.
Xu, K., C. K. Harris, R. D. Hetland, and J. M. Kaihatu (2011), Dispersal of Mississippi and Atchafalaya sediment on the Texas–Louisiana shelf: Model estimates for the year 1993, *Cont. Shelf Res.*, *31*(15), 1558–1575.
Zhang, Y., et al. (2012), Nested-grid simulation of mercury over North America, *Atmos. Chem. Phys. Discuss.*, *12*, 2603–2646.
Zhang, Y., L. Jaeglé, and L. Thompson (2014a), Natural biogeochemical cycle of mercury in a global three-dimensional ocean tracer model, *Global Biogeochem. Cycles*, *28*, 553–570, doi:10.1002/2014GB004814.
Zhang, Y., L. Jaeglé, L. Thompson, and D. G. Streets (2014b), Six centuries of changing oceanic mercury, *Global Biogeochem. Cycles*, *28*, 1251–1261, doi:10.1002/2014GB004939.
Zuo, Z., D. Eisma, and G. W. Berger (1991), Determination of sediment accumulation and mixing rates in the Gulf of Lions, Mediterranean Sea, *Oceanol. Acta*, *14*(3), 253–262.